SOLUTION

# **CUME #393**

Jim Murphy

November 22, 2014

Calculators are to be used ONLY for calculations, not for retrieving constant values.

Write your answers on only a single side of a sheet of paper.

TOTAL # of POINTS AVAILABLE = 65 a priori Passing Grade is  $\sim 65\%$  (42.25 points)

Some possibly useful numeric values:

Mars' orbital velocity on Oct 19, 2014 = 26.0 km per second

Mars' Orbital Semi-major Axis Length = 2.26 x 10<sup>11</sup> meters (=1.52 AU)

Mars' surface gravitational acceleration = 3.72 meters per second per second

Mars' radius = 3395 km

Mars' mass =  $6.4185 \times 10^{23} \text{ kg}$ 

Solar Luminosity =

3.85 x 10<sup>26</sup> W

Gravitational Constant =

6.67 x 10<sup>-11</sup> m<sup>3</sup> kg<sup>-1</sup> s<sup>-2</sup>

Stefan-Boltzmann constant =

 $5.67 \times 10^{-8} \text{ W m}^{-2} \text{ K}^{-4}$ 

Gas constant for  $CO_2 =$ 

189 J kg-1 K-1

Solar escape velocity at 1.5 AU

 $\sim 34 \, \text{km/s}$ 

Sun's mass =

 $2 \times 10^{30} \text{ kg}$ 

Boltzmann's constant =

 $1.38 \times 10^{-23} \text{ J K}^{-1} = 1.38 \times 10^{-16} \text{ ergs K}^{-1}$ 

The questions below are motivated by the accompanying paper, "Perturbation of the Mars atmosphere by the near-collision with Comet C/2013 A1 (Siding Spring)" by Yelle et al. (Icarus, 2014). Questions WILL NOT deal with any chemistry aspects presented in the paper's Section 2.2.

**1)** Decipher the name "C/2013 A1 (Siding Spring)" in the standard form of comet nomenclature [4 points]

C = a COMET, but NOT a periodic comet
2013 = year of detection/discovery
A = first half of the first month of the year, January 1-15
1 = first comet discovered during that half-month
(Siding Spring) - Observatory of discovery

2) Calculate a <u>numerical estimate</u> of Comet Siding Spring's <u>Orbital Semimajor Axis (OSA) length</u> using the information provided in the first paragraph of the accompanying paper. [Note: assume that Siding Spring's direction of travel was 31 degrees of angle away from being directly opposite to Mars' direction of travel.] For this calculation assume that 'Relative velocity' in the paper refers to the effective head-on velocity of the two objects in question.

After you have calculated a numeric OSA value, **comment** on your value and its physical representativeness compared to the text's Introduction description of the comet. [10 points, 7/3]

Mars' orbit speed was 26 km/s. So, Siding Spring's 'head on velocity' was 30 km/s.

Siding Spring's travel was off 31 degrees away from being opposite so Mars' direction, so Siding Spring's full velocity = 30 km/s / (cos 31 degrees) = 35 km/s

Now, 
$$V_{SS} = [GM_{Sun}((2/1.5 AU) - (1/OSA))/1.49 \times 10^{11} \text{ meters}]^{1/2} = 35000 \text{ m/s}$$

for which OSA = -29 AU... and a NEGATIVE OSA is not physical... which is consistent with Siding Spring being a 'hyperbolic' orbiting comet which indicates that on its inbound leg it is not 'permanently' bound to the Sun.. its orbit eccentricity value is greater than 1.0

The solar escape velocity at 1.5 AU is ~34 km/s, so Siding Spring's 35 km/s speed is in excess of the solar escape velocity

- 3) Section 2.1 of the paper discusses the observed 'production rates' of comet nuclei when they are located at a heliocentric distance of 1.4 AU.
- a) **DESCRIBE** two physical processes/conditions that could play a realistic role in causing comet nucleus production rates to exhibit a range of 4 orders of magnitude variation at 1.4 AU among comets. [4 points]

i) comet's that possess a greater ratio of dust-to-ice at their surfaces would be expected to exhibit smaller production rates because less solar flux would go directly into ice heating/sublimation, and an overlying layer of dust above ice can act as an insulating layer as well as a vapor barrier with the net result being smaller magnitude production rates; ii) comets are not all identical in composition; differing water ice abundances would affect the detected sublimation rates,.. some of this can be related to i) above but some also to different dynamical classes of comets with different formation scenarios (different radial distance of formation could affect ices available)

iii) A short period comet would likely arrive at 1.4 AU with a warmer temperature than would a long period comet so there might be a temporal lag for longer-period comet's to achieve as large a production rate as a shorter period ('warmer') comet though the 'lag deposit' discussed below for 4b) could become an issue for shorter period comets

NOTE THAT NUCLEUS SIZE would not itself explain the range of production rates since nucleus sizes range over an order of magnitude but two orders of magnitude would be necessary to account for the 10<sup>4</sup> range in production rate

**b) EXPLAIN** why Jupiter family comets apparently exhibit a tendency to possess 1.4 AU production rates at the smaller magnitude end of the production rate range mentioned in the paper. [3 points]

Jupiter family comets possess small orbital periods (aphelion of ~5.2 AU) and thus experience many periapse sublimation episodes during some finite period of time, making them more likely to have accumulated a surface 'lag' of dusty materials which can inhibit the deposition of sunlight upon ice as well as forming a crust through which sublimed water vapor must diffuse. The paper does make the point that since Siding Spring is a dynamically 'young' comet it can be expected to exhibit a higher-end production rate magnitude.

**4a) CALCULATE** an estimate for Siding Spring's nucleus surface Radiative Equilibrium Temperature when it was located at Mars' distance (1.52 AU) from the Sun; assume no coma was present. State any assumptions you make in setting up and conducting your calculation. [8 points]

$$F_{solar} (1 - Albedo) \pi R_{SS}^2 = 4 \pi R_{SS}^2 \sigma T_{ss}^4$$
  

$$[(601.9 \text{ W m}^{-2}) (0.95) (R_{SS}^2) / (4 \sigma)]^{1/2} = T_{SS}$$

$$T_{ss} = 223 \text{ K}$$

Assumptions: Comet nuclei are dark, so assume low albedo value (0.05)

Assume IR emissivity = 1.0

Assume 'fast rotator'

**b)** Now, <u>qualitatively consider</u> that Siding Spring's nucleus is enveloped in a coma that has a radially integrated optical depth of 1.0 at visible and UV wavelengths. Assume that the coma's opacity is caused only by dust particles that are each 1.0 micrometers in diameter, that the particles' <u>single scattering albedo = 0.9999</u>, and that the particles' <u>asymmetry parameter = 0.0</u>.

For the above described coma conditions, **QUALITATIVELY DESCRIBE** if (and WHY) the resultant Siding Spring nucleus surface Radiative Equilibrium Temperature when at Mars' OSA will be greater than or less than the correct non-coma temperature answer for question 4a) above. [5 points]

The effects of the coma are primarily to scatter solar flux. Since the asymmetry parameter indicates that one-half of the scattered solar flux WILL NOT impinge upon the nucleus (because it will be scattered in the backward direction) the effect of the coma will be to REDUCE the nucleus Equilibrium Temperature since less solar flux will reach the nucleus

c) Now, NUMERICALLY ESTIMATE the <u>scale factor</u> by which the coma effect will change the nucleus' surface Radiative Equilibrium Temperature for the coma conditions described above. Assume each photon is scattered at most only one time. [6 points]

Effect of dust scattering will be to reduce the solar flux reaching the nucleus' surface.. single scattering albedo of 0.999 implies most impinging flux is not absorbed by the coma, and the asymmetry parameter of 0.0 implies equal forward and backward scattering, so....

Unimpeded solar flux getting to surface ~ 1/e ('what gets through unaffected' =  $e^{-\tau}$ )

Scattered flux is  $\sim$ (1 -1/e) and ½ of this gets to the surface, so total flux getting to the surface is:  $1/e + \frac{1}{2}(1 - 1/e) = \frac{1}{2} + \frac{1}{2}e = 0.68$  of what impinged upon the surface without a coma.

Since the Equilibrium Temperature is proportional to  $F_{received}^{0.25}$ , resultant equilibrium temperature is  $0.68^{0.25}$  of the correct value, or 0.9, so  $0.9 \times 223 = 203$  K

**5) Explain** the physical condition which causes the unperturbed Mars atmosphere molecular number density *vs* altitude curves in Figure 3 (**color figure!**) to exhibit different slopes for the different molecular species at altitudes above ~125 km while they exhibit the same slope at altitudes below ~125 km. [**5 points**]

above an altitude of ~125 km atmospheric constituents are no longer well mixed but rather begin to exhibit vertical number density variations that are molecular or atomic weight dependent, so the more massive species exhibit the smallest scale heights/steepest abundance slopes; the atmospheric level below which species are well mixed and above which specie abundances become mass dependent is known as the 'homopause'

# 6) a) WRITE a definition for the 'Atmospheric Scale Height' . [4 points]

Atmospheric Scale Height is the geometric distance within an atmosphere for which the atmospheric pressure (or density) varies by a factor of e or 1/e for downward or upward displacement respectively. This geometric 'thickness' is dependent upon the 'gas constant' of the atmospheric gas, upon the temperature of the gas, and upon the local gravitational acceleration.

Scale Height,  $H = R_{gas} T/g$  with resultant units in meters for input values in the mks system

**b)** The solid curve in Fig 2 displays the atmospheric temperature structure for 'unperturbed' atmosphere conditions, and the authors indicate that a nucleus production rate of  $10^{27}$  s<sup>-1</sup> does not noticeably perturb the atmosphere (end of page 207).

Use the information provided in Figure 11 to **CALCULATE** the <u>average atmospheric temperature in the 150-250 km altitude range</u> that would correspond to a Siding Spring nucleus production rate of  $5 \times 10^{28} \, \text{s}^{-1}$ . The atmospheric density at 150 km altitude is an unchanging value of  $1.13 \times 10^{-9} \, \text{kg m}^{-3}$ .

The difference between the correct calculated temperature and 200 K is an indication of the effect of the comet coma's interaction with Mars' atmosphere. [6 points]

250 km density for  $10^{28}$  s<sup>-1</sup> production rate =  $7 \times 10^{13}$  kg m<sup>-3</sup>

$$ho(250 \text{ km}) = 
ho(150 \text{ km}) e^{-(\Delta_Z/H)}$$
 $7 \times 10^{-13} \text{ kg m}^{-3} = 1.13 \times 10^{-9} \text{ kg m}^{-3} e^{-(100000 \text{ m}/H)}$ 
 $H = 1.35 \times 10^4 \text{ m}$ 

$$H = R_{CO2} \, T \, / g \ , \ \ so \ T = [1.35 \, x \, 10^4 \, m \, x \, (3.72 \, m \, s^{-2}) \, / \, 189 \, J \, kg^{-1} \, K^{-1}] = 266 \, K$$

This assumes that  $CO_2$  remains the dominant gas.. but as is indicated in Figure 3  $CO_2$  dominated only up to ~200 km, and thereafter O2 becomes important. Indication of this gaseous change and its effect upon the calculation was positively taken into account for grading.

**7a)** The concept of **Jean's Escape** from Mars' atmosphere is invoked in the paper (*first complete paragraph on page 205 and the final paragraph on that page, and beneath Fig. 2 on page 206*), as is as the concept of the 'exobase' (*to the left of Fig 2 on page 206*).

**PROVIDE DESCRIPTIONS** of Jean's Escape and the exobase, being sure to mention the important physical processes they account for. [6 points]

Jean's Escape describes thermal 'evaporation' of atoms or molecules from an atmosphere, and is based upon a populations' Boltzmann distribution of thermal velocities and the percentage of those speeds that exceed the escape velocity (in this instance Mars' escape velocity). Now, such 'escape' can be inhibited by collisions with other atoms or molecules,... the 'exobase' defines that level in the atmosphere where the mean-free path of atoms or molecules is equal to or exceeds the atmospheric scale height. this situation statistically indicates that loss-minimizing collisions are unlikely and escape will occur for upward moving species possessing thermal speed equal to or greater than the escape velocity

**b)** Briefly **DESCRIBE** how these same concepts of Jean's Escape and exobase can be applied to the comet nucleus and coma conditions discussed in this paper. [4 points]

Production of the coma involves gaseous 'escape' from the nucleus.. those molecules must have velocity values greater than the nucleus' escape velocity.. at a temperature near 200 K thermal velocity of a water molecule is ~500 m/s which will greatly exceed the nucleus' escape velocity; most if not all of the gaseous molecules substantially exceed the nucleus' escape velocity and since gas densities are small in the coma the surface of the nucleus is equivalent to the 'exobase' for the comet



Contents lists available at ScienceDirect

# Icarus

journal homepage: www.elsevier.com/locate/icarus



# Perturbation of the Mars atmosphere by the near-collision with Comet C/2013 A1 (Siding Spring)



Roger V. Yelle a,\*, A. Mahieux a,b, S. Morrison a, V. Vuitton c, S.M. Hörst d

- <sup>a</sup> Department of Planetary Sciences, University of Arizona, 1629 E. University Blvd., Tucson, AZ 85721, United States
- b Belgian Institute for Space Aeronomy, 3 avenue Circulaire, 1180 Brussels, Belgium
- <sup>c</sup>Institut de Planétologie et d'Astrophysique de Grenoble, Université J. Fourier, Grenoble, France
- <sup>d</sup> Cooperative Institute for Research in Environmental Sciences, University of Colorado, Boulder, CO 80309, United States

#### ARTICLE INFO

Article history: Received 1 January 2014 Revised 17 March 2014 Accepted 19 March 2014 Available online 2 May 2014

Keywords: Mars Comets Atmospheres, structure

## ABSTRACT

The martian upper atmosphere could be strongly perturbed by the near collision with Comet C/2013 A1 (Siding Spring). Significant mass and energy will be deposited in the upper atmosphere of Mars if the comet coma is sufficiently dense. We predict that comet  $H_2O$  production rates larger than  $10^{28}$  molecules/s would produce temperature increases exceeding 30 K and the H density in the upper atmosphere will approximately double. The temperature perturbation will persist for several hours and the increased H density for tens of hours. Drag on orbiting spacecraft may increase by substantial factors, depending upon comet activity, because of the thermal perturbation to the atmosphere. Observation of these perturbations may provide insight into the thermal and chemical balances of the atmosphere.

© 2014 Elsevier Inc. All rights reserved,

#### 1. Introduction

Comet C/2013 A1 (Siding Spring) will have a close encounter with Mars on October 19, 2014. Traveling on a highly inclined. 129°, hyperbolic orbit, this comet will encounter Mars with a relative velocity of about 56 km s<sup>-1</sup> and a close approach distance between 116,000 and 169,000 km [JPL Small-Body Database]. The extended coma will impinge upon the upper atmosphere of Mars for about 1 h. The flux of mass and energy incident upon the atmosphere will be considerable if the comet is active. This provides the opportunity to study the upper atmosphere of Mars at a unique time that could provide insight into physical processes that are difficult to investigate in normal circumstances. The effects of a cometary impact on Jupiter have been well studied (Harrington et al., 2004), but the physical consequences of the transit of a planet through a cometary coma have not previously been examined. Moreover, the near-collision with Siding Spring may affect the atmosphere so that the set of spacecraft currently investigating Mars may view a perturbed rather than normal atmosphere. This is especially important for the MAVEN mission, whose focus is the upper atmosphere of Mars.

Cometary coma contain both dust and gas. Exogenic dust incident upon a planet will penetrate to the level where friction

with the ambient atmosphere heats the dust to its melting point. Typically, disintegration of the dust occurs at pressures on the order of a  $\mu bar$ , in the mesosphere. Gas molecules will be deposited at much higher levels, where ambient densities are much lower, and the potential for significant atmospheric perturbations much higher. The depth of penetration for the gas molecules can be estimated from their stopping power, which depends on their energy. Cometary coma at 1.4 AU are predominantly  $H_2O$ . The kinetic energy of an  $H_2O$  molecule at  $56~{\rm km~s^{-1}}$  is 293 eV. We estimate in the next section that  $H_2O$  molecules with this energy will penetrate to a column abundance of  ${\sim}5\times10^{15}~{\rm cm^{-2}}$ . For a input angle of 60 degrees, this column density corresponds to a pressure of  $6.5\times10^{-5}~\mu bar$  and an altitude of  $154~{\rm km}$  for nominal atmospheric conditions. This is in the topside ionosphere, in the heart of the martian thermosphere.

We consider here the effects of this gaseous input from the comet coma on the thermosphere of Mars. This rare event may have both practical and scientific consequences. The time scale of the atmospheric response to the perturbation is directly connected to physical processes controlling the upper atmospheric structure. Observing the time-dependent response to a perturbation provides different insight on the physical processes than is revealed in investigations of steady state structure. For example, we show that the time scale for removal of the H added to the martian atmosphere depends sensitively on the eddy diffusion coefficient, an important but uncertain parameter in all models for the Mars upper atmosphere. In terms of practical consequences, we show

<sup>\*</sup> Corresponding author.

E-mail addresses: yelle@lpl.arizona.edu, rogeryelle@gmail.com (R.V. Yelle).

that, for a sufficiently dense coma, heating of the atmosphere may raise densities at high altitudes thereby increasing drag on orbiting spacecraft. This may be important for the spacecraft. In addition, it may be the simplest way to measure the thermal time constant for the response to the perturbation.

In order to address these questions we first consider the characteristics of the energy and mass input to the atmosphere. We then describe 1D atmospheric models that provide quantitative estimates of the atmospheric response to the perturbations. The results of the models and the implications for observations are discussed in Sections 4 and 5.

#### 2. Mass and energy deposition

The thermosphere of Mars is rich in O and it is unlikely that the contributions from the comet could significantly alter the O inventory. The H abundance in the unperturbed atmosphere is much smaller and the cometary contribution can be significant. Temperatures can also be strongly affected because of the large kinetic energy of the impacting molecules. In the calculations that follow we consider perturbations of both H density and temperature in the Mars upper atmosphere caused by the influx of cometary  $\rm H_2O$ .

#### 2.1. Mass and energy fluxes

The flux of mass and energy into the martian atmosphere depends on the activity of the comet, most conveniently described by the  $\rm H_2O$  production rate. Production rates of observed comets vary widely from  $10^{26}$  to  $10^{30}$  molecules  $\rm s^{-1}$  at 1.4 AU, with a tendency for Jupiter family comets to have lower rates (A'Hearn et al., 1995; Fink, 2009). Siding Spring is a dynamically new comet and the rate may be significant. We show that rates below  $10^{27} \, \rm s^{-1}$  have little effect on the martian atmosphere and for rates larger than  $10^{29} \, \rm s^{-1}$  the perturbation to the atmosphere is so extreme that the models used here are probably no longer valid; thus, we consider production rates in the  $10^{27} - 10^{29}$  range in our calculations.

We adopt a simple model for the spherical expansion of the coma to estimate the fluxes incident upon the atmosphere. With this model the  $\rm H_2O$  number density at a distance  $\it r$  from the nucleus is

$$N = \frac{P}{4\pi r^2 U},\tag{1}$$

where P is the  $H_2O$  production rate and U the outflow velocity of the coma. The flux of H into the atmosphere is

$$F_H = 2VN = \frac{PV}{\pi r^2 U},\tag{2}$$

and the flux of energy

$$F_{E} = \frac{1}{2} m_{\rm H_{2}O} V^{3} N = \frac{m_{\rm H_{2}O} P V^{3}}{2\pi r^{2} U}. \tag{3}$$

Adopting a production rate of  $P=10^{28}~\rm s^{-1}$  as a typical value,  $U=1~\rm km~s^{-1}$  (Tenishev et al., 2008), and  $r=130,000~\rm km$  and  $V=56~\rm km~s^{-1}$  for the separation and relative velocity between Siding Spring and Mars gives values at the closest approach of  $N=47~\rm cm^{-3}$ ,  $F_H=5.2\times10^8~\rm cm^{-2}~s^{-1}$ , and  $F_E=1.2\times10^{-1}~\rm erg$  cm<sup>-2</sup> s<sup>-1</sup>. The time-integrated values for the H and energy input are  $3.7\times10^{12}~\rm cm^{-2}$  and  $8.7\times10^2~\rm erg~cm^{-2}$ .

We are not aware of any quantitative information on the collision rates or products for a 300 eV collision between  $\rm H_2O$  and  $\rm CO_2$  molecules; therefore, we base our discussion on some general principles. The kinetic energy of the impacting  $\rm H_2O$  is well above the dissociation and ionization energies of the molecule. Possible products of collisions include  $\rm H_2O^+$ , H, OH, H $^+$ , OH $^+$ , and OH $^-$ . Repeated

collisions could results in further fragmentation. As ions travel through the martian atmosphere they lose energy both through electronic excitations and momentum transfer to the ambient molecules, primarily CO<sub>2</sub>. The altitude of deposition is determined by the stopping power, given by

$$\frac{dE}{dX} \approx N_b(S_e + S_n),\tag{4}$$

where  $S_e$  and  $S_n$  are the electronic and nuclear stopping cross sections and  $N_b$  is the density of molecules encountered (Johnson, 1990). We estimate the stopping power from empirical equations that match experimental measurements at higher energies (10-10<sup>5</sup> keV) (Johnson, 1990; Ziegler, 1980, 1984), as measurements below 1 keV are not available. The stopping power is then used to calculate the column abundance required to stop the oxygen ions. Our calculations of the stopping power of CO<sub>2</sub> for O<sup>+</sup> ions is shown in Fig. 1. These should also be approximately correct for H2O+, OH+ or OH- because the calculations depend primarily on mass and the mass of these ions is similar. A rough estimate for the range of the ions can be obtained from the ratio of the original energy to the stopping power,  $300 \text{ eV}/6 \times 10^{-14} \text{ eV cm}^{-2} \sim 5 \times 10^{15} \text{ cm}^{-2}$ . H fragments from the precipitating molecules will have less energy because of their smaller mass and therefore have a smaller range, We assume that the H atoms are carried along with the heavier O atom to the deposition altitude, when in fact some of the H may be deposited at a significantly higher altitude. The errors associated with this assumption are unlikely to be larger than a factor of 2 and therefore are tolerable for this initial study.

#### 2.2. Chemical considerations

We assume that the exogenic hydrogen reaches thermal energies in the martian upper atmosphere in the form of H<sup>+</sup>, OH<sup>+</sup> and H<sub>2</sub>O<sup>+</sup> and consider the chemical fate of these ions. Our discussion of the chemistry is based on the compilations of ion-molecule reactions by Anicich (1993) and McEwan and Anicich, 2007, the compilations of Baulch et al. (2005) and Sander et al. (2011) for neutral chemistry and the online database KIDA (Wakelam, 2012, http://kida.obs.u-bordeaux fr) unless mentioned otherwise. Below 200 km, the five most abundant neutral species of the martian atmosphere are CO<sub>2</sub>, CO, O, N<sub>2</sub> and Ar. As an inert gas and it can be safely assumed that Ar does not play any role in the chemistry. H<sup>+</sup> does not react with either N<sub>2</sub> or CO and the chemistry is initiated by its interaction with CO<sub>2</sub> and O according to the following reactions:

$$H^{+} + CO_{2} \rightarrow HCO^{+} + O$$
 (R1)  
 $H^{+} + O \rightarrow O^{+} + H$  (R2)

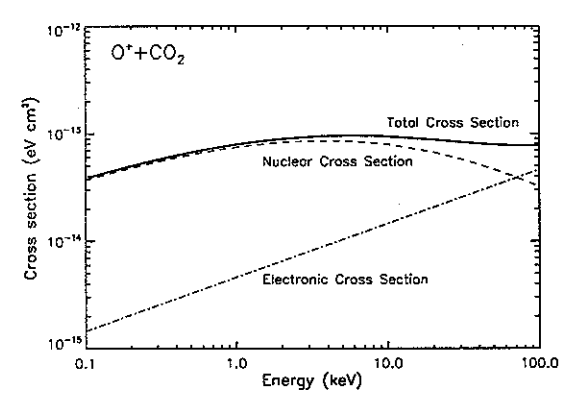


Fig. 1. The stopping power of CO2 for O+ ions.

The importance of these reactions has been emphasized by Matta et al. (2013). OH\* is reactive with all major martian neutral species and in this case, hydrogen is transferred into the OCOH\*,  $N_2H^*$  and  $HCO^*$  ions:

$$OH^{+} + CO_{2} \rightarrow OCOH^{+} + O$$

$$OH^{+} + N_{2} \rightarrow N_{2}H^{+} + O$$

$$(R3)$$

$$(R4)$$

$$OH^{+} + CO \rightarrow HCO^{+} + O$$

$$(R5)$$

$$OH^{+} + O \rightarrow RCO^{+} + O$$

$$OH^{+} + O \rightarrow O_{2}^{+} + H$$
(R6)

 $H_2O^*$  does not react with either  $CO_2$ ,  $N_2$  or O but it does with CO according to the following reaction:

$$H_2O^+ + CO \rightarrow HCO^+ + OH$$
 (R7)

OH\* and H<sub>2</sub>O\* are also at the origin of H atoms and to a much lesser extent H<sub>2</sub>, through electron dissociative recombination (Mul et al., 1983; Mitchell, 1990; Rosén et al., 2000):

$$OH^{+} + e^{-} \rightarrow O + H$$
 (R8)

$$H_2O^+ + e^- \rightarrow O + H + H$$
 (R9a)

$$\rightarrow OH + h,$$
 (R9b)

$$\rightarrow O + H_2, \qquad \qquad \qquad$$
 (R9c)

Therefore, the new species created in reactions (R1)–(R7) include the  $N_2H^+$ , OCOH<sup>+</sup> and HCO<sup>+</sup> ions, while reactions (R8) and (R9a-b) essentially lead to production of H atoms.

N<sub>2</sub>H<sup>+</sup> formed in reaction (R4) is a secondary source of OCOH<sup>+</sup> and HCO<sup>+</sup> according to the following reactions:

$$N_2H^+ + CO_2 \rightarrow OCOH^+ + N$$
 (R10)

$$N_2H^+ + CO \rightarrow HCO^+ + N_2 \qquad (R11)$$

It can also be transformed into neutral species by dissociative electron recombination,

$$N_2H^+ + e^- \rightarrow N_2 + H \tag{R12a}$$

 $\rightarrow$  NH + N, (R12b)

essentially H atoms as far as hydrogen is concerned, (R12b) being a marginal channel. OCOH\* formed in reaction (R3) and (R10) is converted to the end product of the ion chemistry, HCO\*,

$$OCOH^+ + CO \rightarrow HCO^+ + CO_2$$
 (R13)

$$OCOH^+ + O \rightarrow HCO^+ + O_2$$
 (R14)

and to H and OH via electron recombination:

$$OCOH^+ + e^- \rightarrow CO \neq O + H$$
 (R15a)

$$\rightarrow$$
 CO + OH (R15b)

$$\rightarrow CO_2 + H$$
 (R15c)

Finally, HCO\* formed in reactions (R1), (R5), (R7), (R11), (R13) and (R14) does not react with any of the major constituents of the martian atmosphere and its fate is to recombine with electrons:

$$HCO^{+} + e^{-} \rightarrow CO + H$$
 (R16a)  
 $\rightarrow C + OH$  (R16b)  
 $\rightarrow O + CH$  (R16c)

The H in HCO $^{+}$  is therefore mostly converted to H atoms and to some lower extent to OH, channel (R16c) being negligible (Le Padellec et al., 1997; Geppert et al., 2005). Therefore, the ultimate fate of H $^{+}$ , OH $^{+}$  and H $_{2}$ O $^{+}$  ions on Mars is to be converted to H atoms and a smaller fraction of OH radicals, via the formation of  $W_{2}$ H $^{+}$ , OCOH $^{+}$  and HCO $^{+}$  and their subsequent dissociative electron recombination products.

Interestingly, the reactivity of H atoms with the major atmospheric constituents, CO<sub>2</sub> and N<sub>2</sub>, is extremely weak (Baulch

et al., 2005; Caridade et al., 2005). H atoms can react with CO and O, 
$$H + CO \rightarrow HCO$$

$$H + O \rightarrow OH.$$
(R17)

but these are association reactions that require a three-body collision or radiative emission of a photon to be fast. On Mars, three-body collisions can only occur at the very lowest altitudes and, because of the small number of atoms in these molecules, radiative association is expected to be inefficient (Vuiton et al., 2012); thus, reactions R17 and R18 are not expected to be important in the martian upper atmosphere. Even if some H atoms are converted to HCO and OH through reactions (R17) and (R18), these species ultimately form back H, through the following set of reactions:

$$HCO + O \rightarrow CO_2 + H$$
 (R19a)  
  $\rightarrow CO + OH$  (R19b)

$$OH + CO \rightarrow CO_2 + H$$
 (R20)

$$OH + O \rightarrow O_2 + H \qquad (R21)$$

OH<sup>-</sup> is another possible product of the H<sub>2</sub>O precipitation. The chemistry of OH<sup>-</sup> is not nearly as well constrained as that of H+, as is always the case when it comes to negative ions (Vuitton et al., 2009). Several types of reactions can be envisioned, such as ion-neutral reactions, charge exchange reactions, associative detachment, ion-ion recombination and photodetachment. Although relevant reactions for the martian atmosphere are not available, it seems likely that the H in OH<sup>-</sup> is converted to H, OH of HCO and therefore ultimately ends up as H atoms, as discussed above.

#### 2.3. Implications for the atmosphere

In summary, the precipitating H2O molecules should penetrate to the  $\sim$ 150 km level, depositing energy, H, and O atoms. H atoms are stable in the upper atmosphere and can only be lost by diffusion to the exosphere or lower atmosphere. Over the lifetime of the influx, approximately  $3.7 \times 10^{12}$  cm<sup>-2</sup> H atoms and  $8.7 \times 10^2$  erg cm<sup>-2</sup> will be deposited in the atmosphere. The abundance of H and thermal energy in the unperturbed atmosphere above 150 km are  $1.1 \times 10^{12}$  cm<sup>-2</sup> and  $1.8 \times 10^{2}$  erg cm<sup>-2</sup>; thus, the cometary input may significantly perturb both the H and energy balance in the atmosphere. The transport of heat and minor constituents in the upper atmosphere are dominated by diffusion and the time constant for these processes can be estimated from  $t_{\rm D} \sim H^2/K$ , where K is the eddy diffusion coefficient, which we use here to estimate the diffusion rate in the upper atmosphere. Adopting typical values of H = 13 km and  $K = 10^8 \text{ cm}^2 \text{ s}^{-1}$  (Nair et al., 1994) gives  $t_D \sim 4.5 \text{ h}$ , a factor of several longer than the coma interaction time of  $\sim$ 1 h. Thus the cometary input is comparable to the inventory of H atoms and energy in the upper atmosphere and is deposited over a period of time short compared with the vertical transport times. As a consequence, we expect considerable perturbation of the upper atmosphere for a sufficiently active comet.

#### 3. Model description

We study the perturbations from the comet with a 1D time-dependent model for the upper atmosphere. There will, of course, be 3D effects that can only be simulated by a GCM, but these are neglected for this exploratory study. The differences between 1D and 3D simulations can be factors of several in terms of heating rate and constituent densities, which are considerable, but the

current uncertainty on the cometary production rate is several orders of magnitude. A 1D model allows us to investigate, without too much computational overhead, the likely effects of the near collision and should point the way to more precise simulations should the effects prove interesting.

Our 1-D model of the martian upper atmosphere calculates temperature and composition by solving the coupled, time-dependent energy balance, diffusion, and continuity equations. The model domain covers the 100–250 km altitude region at a resolution of 1 km. We fixed the pressure at the lower boundary of the model atmosphere to 0.05 µbar. We treat the atmosphere as plane-parallel and hydrostatic, but allow H to diffuse through the background atmosphere and to escape. We consider only thermal escape at the Jeans rate. We calculate both steady-state solutions and time-dependent solutions in response to the variable cometary input. The time-dependent solutions are calculated with a Crank-Nicholson integration scheme. The steady-state solutions are derived from the same model but without comet input and run until time derivatives are insignificant.

The mean thermal state of the martian upper atmosphere can be understood as a balance among heating due to absorption of solar EUV and near IR radiation, thermal conduction, and radiative cooling from the  $v_2$  bending mode of  $CO_2$ , excited primarily by collisions with atomic oxygen (Bougher et al., 1999, 2000, 2002). The time-dependent thermal balance equation is:

$$\rho c_p \frac{\partial T}{\partial t} = Q_{UV} + Q_{NIR} + Q_{FIR} + Q_{COM} + \frac{\partial}{\partial \tau} k_T \frac{\partial T}{\partial \tau}$$
(5)

where Q<sub>IV</sub> represents solar UV heating and is obtained by calculating atmospheric absorption of solar radiation at wavelengths shorter than 200 nm with a uniform heating efficiency of 20% (Huestis et al., 2008). We use TIMED/SEE Level 3 solar spectral irradiance data taken on 19 June 2013 during moderate solar conditions to represent solar output (Woods et al., 2005). CO2 absorption cross sections are obtained from Parkinson et al. (2003) and were measured at a temperature of 195 K, quite close to the temperatures in the Mars upper atmosphere. Calculations are performed on a wavelength grid with 1 nm spacing. Q<sub>NIR</sub> represents solar heating in the near IR bands of CO2 at 4.3 μm, 2.7 μm and shorter wavelengths (Lopez-Puertas and Lopez-Valverde, 1995). We do not calculate this rate from first principles however, but rather parameterize it as a constant times the square of the CO<sub>2</sub> density with the constant adjusted to give a temperature of 120 K at the base of our model. This heat source is only important near the base of our atmospheric model and more complex calculations are not warranted because our focus is on higher altitudes in the thermosphere. The last term on the RHS of Eq. (5) represents heating due to the divergence of the thermal conduction flux with  $k_T$ , the thermal conduction coefficient, calculated as the weighted average of conductivities for CO<sub>2</sub> (Vesovic et al., 1990) and O (Dalgarno and Smith, 1962). Q<sub>COM</sub> represents the heating rate associated with the comet and is set to zero for the steady-state simulations.

The radiative cooling rate,  $Q_{FIR}$  is derived from the excitation of the 15  $\mu m$  bending mode of  $CO_2$  resulting from collisions with other  $CO_2$  molecules or with atomic oxygen, neglecting subsequent re-absorption and re-emission:

$$Q_{FIR} = -h\nu \frac{A_{10}C_{10}}{A_{10} + C_{10}} \frac{g_1}{g_0} N(CO_2) \exp\left(-\frac{h\nu}{kT}\right)$$
 (6)

where  $A_{10}=1.35~{\rm s}^{-1}$  is the Einstein transition probability for the  $v_2$  band of CO<sub>2</sub>,  $C_{10}$  is the collisional de-excitation rate for the excited state, and  $g_1/g_0=2$  is the ratio of the statistical weights for the excited and ground states. The collisional de-excitation rate is given by

$$C_{10} = k_0 N(0) + k_{CO_2} N(CO_2)$$
 (7)

where  $k_0$  and  $k_{CO_2}$  are the rate coefficients for collision de-excitation of  $CO_2$  by O and  $CO_2$  respectively. De-excitation by collisions with O is far more efficient than for collisions with  $CO_2$  and the latter can be neglected without affecting the solution. Though  $k_0$  is fast, the rate is uncertain. Successful Mars GCMs adopt a value of  $3\times 10^{-12}$  cm³ s<sup>-1</sup> (Bougher et al., 1999, 2000; González-Galindo et al., 2005), but the most recent laboratory measurement finds a value of  $1.5\times 10^{-12}$  cm³ s<sup>-1</sup> (Castle et al., 2012). In contrast, analysis of satellite observations of  $CO_2$  15  $\mu$ m band limb emissions in the terrestrial atmosphere by Feofilov et al. (2012) require a value of  $6\times 10^{-12}$  cm³ s<sup>-1</sup>. Our reference model uses a value of  $3\times 10^{-12}$  cm³ s<sup>-1</sup> in accord with other Mars studies, but we also examine how atmospheric temperatures depend on this parameter.

The density profiles are calculated by solution of the timedependent continuity equation

$$\frac{\partial N_i(z,t)}{\partial t} = P_i(z,t) - \frac{\partial \Phi_i(z,t)}{\partial z},\tag{8}$$

where the flux,  $\Phi_i(z,t)$  is given by

$$\Phi_{i}(z,t) = -D_{i} \left[ \frac{\partial N_{i}(z,t)}{\partial z} + N_{i}(z,t) \left( \frac{1}{H_{i}} + \frac{(1+\alpha_{i})}{T} \frac{\partial T}{\partial z} \right) \right] 
- K \left[ \frac{\partial N_{i}(z,t)}{\partial z} + N_{i}(z,t) \left( \frac{1}{H_{a}} + \frac{1}{T} \frac{\partial T}{\partial z} \right) \right].$$
(9)

In these equations  $N_i(z,t)$  is the density of the *i*th species,  $P_i$  is the production rate due to cometary input, T is the temperature,  $H_i = kT/m_ig$  is the scale height of the *i*th species in the diffusion dominated region of the atmosphere,  $D_i$  is the diffusion coefficient for the *i*th species calculated from

$$D_i = \left(\sum_{j \neq i} \frac{N_j}{b_{ij}}\right)^{-1} \tag{10}$$

where the sum is over the main constituents of the martian upper atmosphere ( $CO_2$  and O) and  $b_{ij}$  are the binary diffusion parameters, with a temperature dependence given by  $b=AT^s$ . We adopt values of (A, s) = ( $5.51 \times 10^{16}$ , 0.841), ( $4.87 \times 10^{17}$ , 0.841) and ( $5.70 \times 10^{17}$ , 0.708) for O-CO<sub>2</sub>, H-CO<sub>2</sub>, and H-O. These values are taken from-Bank et al. (1973). The value for O-CO<sub>2</sub> is assumed equal to that for O-Ar, the value for H-CO<sub>2</sub> is assumed equal to that for H-N<sub>2</sub>. Binary diffusion parameters for H are rarely measured and the values quoted above are estimated based on measured values for self diffusion. The parameter  $\alpha$  in Eq. (9) is the thermal diffusion factor, assumed equal to 0 for O and -0.25 for H. The eddy diffusion coefficient K in the reference model is assumed to be equal to a constant value of  $10^8$  cm<sup>2</sup> s<sup>-1</sup> for the reference model (Nair et al., 1994), but we also consider smaller and larger values.

The distribution of O is calculated by specifying a mole fraction at the lower boundary. Our reference model adopts a value of  $5 \times 10^{-3}$ , which produces a density at the exobase of  $10^7$  cm<sup>-3</sup> that agrees with the value determined from analysis of observations of the OI resonance line at 130.4 nm (Stewart et al., 1992; Chaufray et al., 2009). The escape flux of O from the top boundary is set to 0 because the Jeans escape velocity for O is infinitesimal. For H we utilize two different boundary conditions, depending upon the simulation. For the atmosphere unperturbed by cometary input we fix the H mole fraction at the lower boundary to a value of  $2.5 \times 10^{-6}$ , which produces a density at 250 km of  $1 \times 10^{5}$  cm<sup>-3</sup> consistent with values determined from observations of H Lyman alpha emissions (Chaufray et al., 2008) for the cold, dominant population of H at the exobase. This lower boundary condition represents a source of H in the lower atmosphere, ultimately from H<sub>2</sub>O photolysis, that diffuses to the upper atmosphere. When calculating the effects of cometary input however, we set the altitude derivative of H density to zero at the lower boundary. This represents H deposited in the upper atmosphere diffusing to the lower atmosphere at the fastest possible rate. The H deposited in the upper atmosphere will diffuse to the lower atmosphere because the cometary input is too small to alter the H density in the atmosphere as a whole, it can only perturb the inventory in the less dense upper atmosphere. Thus, the enhancement of H in the upper atmosphere creates a gradient in the H moie fraction that drives a downward flux. The H also diffuses upward to the exobase where it is subject to escape. Here we adopt as an upper boundary condition that H escape at the Jeans velocity for both steady-state and time-variable simulations. The H distribution in the cometary input models is the sum of the steady-state solutions with the fixed density fraction boundary condition and the timevariable solutions with the fixed gradient boundary condition. This is permissible as long as H is a minor component of the upper atmosphere. In this situation, the problem is linear in the H density and solutions due to the different sources of H can be combined with simple addition.

The pressure distribution in the atmosphere is assumed to be hydrostatic at each time step. The time constant to re-establish hydrostatic equilibrium is roughly the atmospheric scale height divided by the sound speed, or  $\sim\!30\,\mathrm{s}$ , which is small compared with the interaction time of  $\sim\!1$  h. The total atmospheric density is obtained from pressure using the ideal gas law. This, combined with solutions to Eq. (9), provides the mole fractions of all constituents, the mean molecular weight of the atmosphere, and completes specification of the atmospheric parameters.

Because of the uncertainties in the mass and energy deposition profiles we model them in a simple way, adopting Chapman-like profiles:

$$Q_{COM} = Q_o N \exp(-\sigma \eta/\mu_o)$$
 (11)

$$P_{H} = P_{\circ} N \exp(-\sigma \eta / \mu_{\circ}) \tag{12}$$

where N is the local atmospheric number density,  $\eta$  is the overhead atmospheric column density, and  $\mu_{\sigma}$  the average cosine of the incidence angle. The parameters  $Q_{\sigma}$  and  $P_{\sigma}$  are adjusted so that the column-integrated heating and H production rates are equal to the (time-dependent) incident fluxes in Eqs. 2 and 3. The peak altitude for this profile is determined by the effective cross section  $\sigma$ . Eased on the discussion of stopping power above, we adopt  $\sigma=2\times10^{-15}$  cm² for the calculations presented here.

The coma of Siding Spring will rain down over essentially one hemisphere on Mars. The sub-comet latitude and west longitude at the time of closest approach are  $-8.6^{\circ}$  and  $22.4^{\circ}$ , corresponding to a solar local time of 5:30 AM, just before dawn. The bombarded hemisphere is therefore roughly half illuminated. In order to model the average effects of the cometary input over the bombarded hemisphere we adopt  $\mu_o = 1/2$  and scale the H production rates and heating rates by 1/2, the ratio of the projected area to the surface area of one hemisphere. In adopting this value we are assuming that the mass and energy deposited by the comet stay primarily in the sub-comet hemisphere, i.e. that both H and energy are transported vertically rather than horizontally over the time scale of the encounter. The alternate assumption, that horizontal transport dominates, would imply a scaling factor of  $\frac{1}{4}$ . Finally, we note that the heating efficiency of 293 eV H<sub>2</sub>O molecules is unknown and we adopt value of 50%. With these assumptions, an H<sub>2</sub>O production rate of 10<sup>28</sup> s<sup>-1</sup> translates to a columnintegrated H deposition rate of 2.8 × 108 cm<sup>-2</sup> s<sup>-1</sup> and a columnintegrated heating rate of 0.03 erg cm<sup>-2</sup> s<sup>-1</sup> at closest approach.

#### 4. Results

Fig. 2 shows temperature profiles for our steady-state model for several values of  $k_0$ . For these calculations we assume a solar

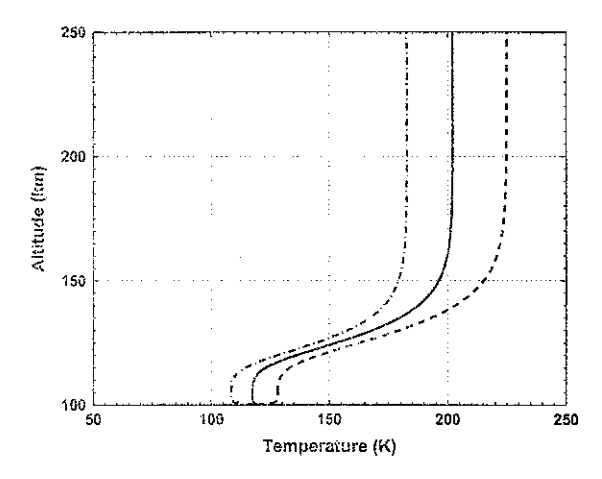


Fig. 2. Temperature profiles of model unperturbed atmospheres for three different  $0-CO_3$  de-excitation rates. The solid, dashed, and dot-dashedlines corresponds to  $0-CO_2$  de-excitation rates of  $3.0\times10^{-12}$  cm<sup>3</sup> s<sup>-1</sup>,  $1.5\times10^{-12}$  cm<sup>3</sup> s<sup>-1</sup>, and  $6.0\times10^{-12}$  cm<sup>3</sup> s<sup>-1</sup>,

zenith angle of  $60^\circ$  and scale heating rates by  $\frac{1}{2}$  to represent a global average. The density profiles corresponding to the reference model of  $k_0 = 3 \times 10^{-12} \ \mathrm{cm^{-2}\ s^{-1}}$  are shown in Fig. 3. The calculated exospheric temperature of 202 K for the reference model is in rough accord with other atmospheric models and with observations (Bougher et al., 2000; Leblanc et al., 2006) while the temperatures near the lower boundary are near the mean of SPICAM occultation results (Forget et al., 2009). The H escape flux from this model is  $1.7 \times 10^7 \ \mathrm{cm^{-2}\ s^{-1}}$ , which is somewhat smaller than the limiting flux value of  $4.5 \times 10^7 \ \mathrm{cm^{-2}\ s^{-1}}$ . Thus, H escape from this steady-state model is limited primarily by the Jeans velocity at the exobase with a small contribution from diffusion.

Fig. 4 shows the various terms in the energy equation. In steady-state there is a precise balance among all terms, with solar UV heating and the divergence of the thermal conduction flux dominating at most altitudes. Radiative cooling in the  $\nu_2$  band of  $CO_2$  makes a significant contribution at altitudes below 160 km. Heating in the near IR bands of  $CO_2$  is only important in a small altitude range near the lower boundary. The rates calculated here

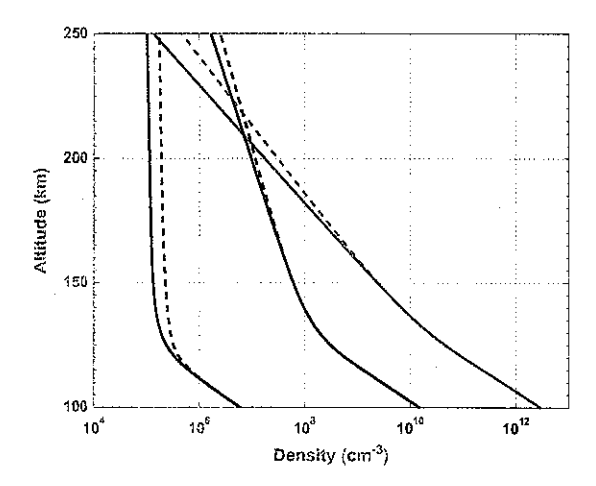
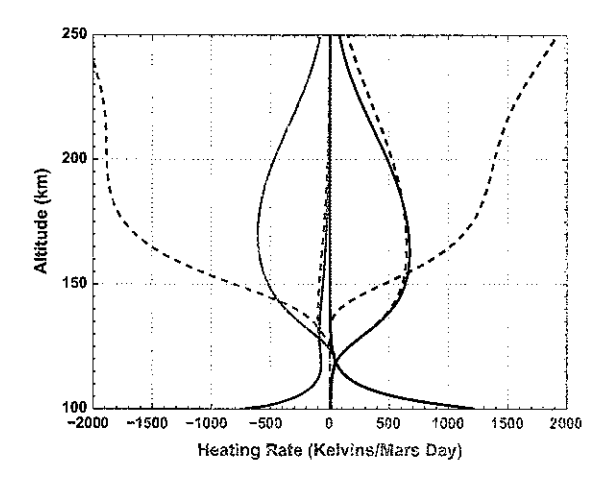


Fig. 3. Profiles of the CO<sub>2</sub>, O, and H density for the unperturbed model atmosphere (solid lines) and a perturbed model for a production rate of 10<sup>28</sup> s<sup>-1</sup> at the time of peak temperature perturbation (dashed lines): CO<sub>2</sub>-green, O-blue, and H-red. (For interpretation of the references to color in this figure legend, the reader is referred to the web version of this article.)



**Fig. 4.** Terms in the energy balance equation for the steady-state atmosphere (solid lines) and perturbed atmosphere (dashed lines) at the time of the peak temperature perturbation:  $Q_{UV}$ -red,  $Q_{EW}$ -green,  $Q_{WW}$ -blue,  $Q_{COW}$ -magenta, and thermal conduction-black. (For interpretation of the references to color in this figure legend, the reader is referred to the web version of this article.)

are in excellent agreement with the results of Bougher et al. (1999) when proper account is taken of diurnal averaging.

Fig. 5 shows the comet's energy flux at Mars and the resulting thermal evolution of the atmosphere for a comet production rate of  $10^{28} \, \mathrm{s}^{-1}$ . Peak temperatures occur 25 min after closest approach and are elevated by about 32 K relative to the unperturbed atmosphere. The heating drops rapidly after the comet passes Mars with a time constant of roughly 1 h; however, the atmosphere's response lags considerably taking about 2.2 h to decrease by a factor of e. As shown in Fig. 4, heating due to the comet is confined to altitudes above  $\sim 150 \, \mathrm{km}$  and is balanced primarily by thermal conduction, which transports the energy downward to  $\sim 130 \, \mathrm{km}$  where it is radiated away by  $\mathrm{CO}_2$ . The temperature profile is

essentially isothermal above 160 km because of the efficiency with which thermal conduction redistributes energy. Temperatures are unperturbed below 130 km because the energy from the comet never reaches those levels.

Fig. 6 shows the evolution of H density in the upper atmosphere. The maximum enhancement in H densities is a factor of 1.8. These are reached approximately 77 min after closest approach. The density perturbation decays away with an e-folding time of 11.8 h. Fig. 7 shows the H flux in the atmosphere for several times during and after the cometary input. During the encounter, H flows primarily upward. For example, at the time of the peak H density perturbation the maximum upward and downward fluxes are  $1.2 \times 10^3 \ \rm cm^{-2} \ s^{-1}$  and  $4.0 \times 10^7 \ \rm cm^{-2} \ s^{-1}$ , respectively. However, it is more difficult to diffuse downward, through higher density, and the downward fluxes persist for a longer time. Integrated over time the net enhancement in the H escape rate due to cometary input is estimated to be  $5 \times 10^{29}$  atoms while  $7 \times 10^{29}$  atoms flow to the lower atmosphere.

The differences in the temporal behavior of temperature and H density are striking. The perturbation to H density persists approximately five times longer than the perturbation to temperature for this model. This is a consequence of the different sinks for energy and H density. The extra heat in the atmosphere is conducted to  $\sim\!130~\rm km$  where it is radiated away, whereas the extra H atoms must diffuse through the lower boundary to, eventually, be lost to chemistry in the lower atmosphere. Thus, although thermal conduction and molecular diffusion have comparable efficiencies, the distance between source and sink for energy is smaller than that for H

The sizes of the temperature and density perturbations depend sensitively on the cometary activity. This is shown in Fig. 8. For an  $\rm H_2O$  production rate of  $10^{27}\,\rm s^{-1}$  the temperature perturbation is only  $\sim 3$  K and the H enhancement only  $\sim 10\%$ . It is likely that these perturbations would be undetectable against the background of normal atmospheric variability. For an  $\rm H_2O$  production rate of  $10^{29}\,\rm s^{-1}$  the temperature perturbation is over 300 K and the H

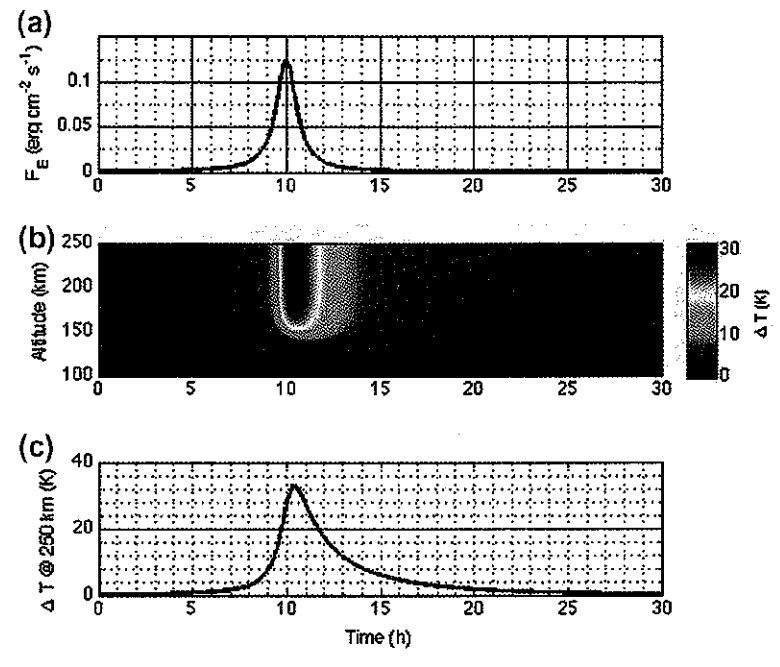


Fig. 5. Calculations of the time evolution of atmospheric temperature for an  $H_2O$  production rate  $10^{28}$  s<sup>-1</sup>. (a) The incident energy flux from the comet as a function of time. (b) The temperature perturbation induced by the cometary input as a function of altitude and time. (c) The temperature perturbation at an altitude of 250 km as a function of time.

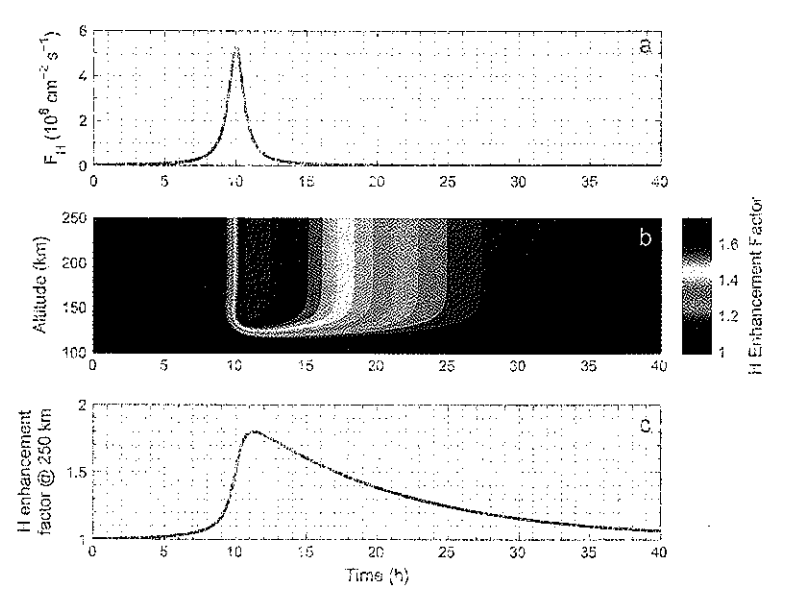


Fig. 6. Calculations of the time evolution of H density for an  $H_2O$  production rate  $10^{28} \, s^{-1}$ . (a) The incident H flux from the comet as a function of time. (b) The ratio of H density in the perturbed atmosphere to the steady-state atmospheric model induced as a function of altitude and time, (c) The ratio of H densities in the perturbed atmosphere at an altitude of 250 km as a function of time.

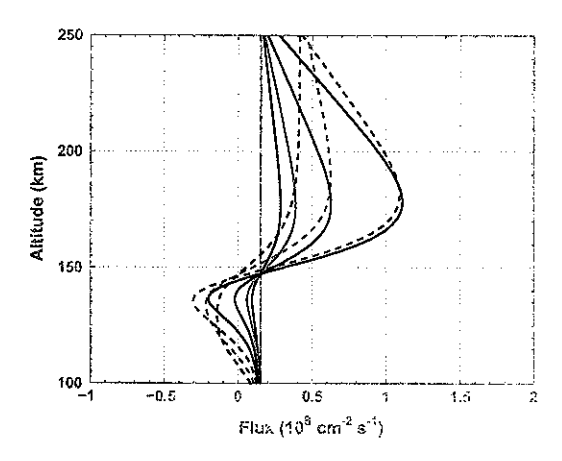


Fig. 7. The H flux in the perturbed atmosphere at the time of closest approach (red), 30 (magenta), 60 (green) and 30 min (blue) from closest approach (magenta). The solid lines are for times before closest, dashed after closest approach. The black curve shows the value of the H flux in the unperturbed atmosphere. (For interpretation of the references to color in this figure legend, the reader is referred to the web version of this article.)

enhancement more than a factor of 3. The temperature and H density perturbation behave differently with increasing cometary input. Temperatures tend to rise rapidly because the increase in temperature causes an increase in scale height resulting in higher altitudes for the energy disposition. This energy must then flow downward over a larger distance to reach the radiative layer. Thermal conduction over this larger distance results in a larger temperature rise. The increased scale height means that the volume of the upper atmosphere also increases. This represents a dilution of the effects of the cometary H and the increase in H density is smaller than it would be if the temperature were to remain constant.

The large temperatures predicted by the models with production rates  $\sim\!10^{29}\,\mathrm{s}^{-1}$  are unlikely to be realistic. Such large temperature differences would produce a pressure gradient that would

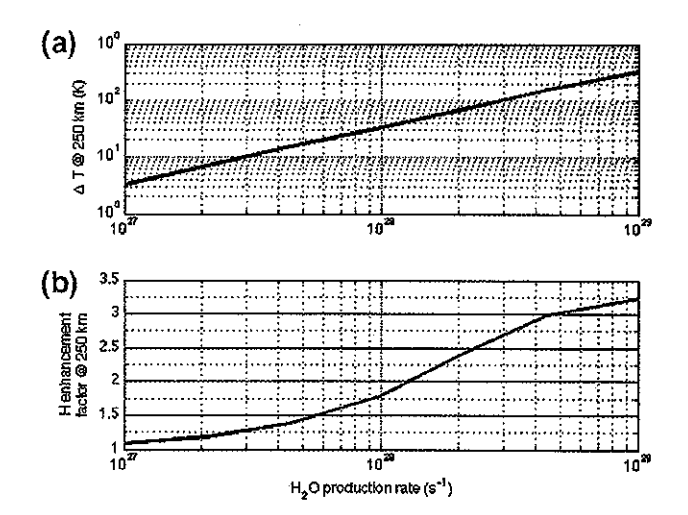
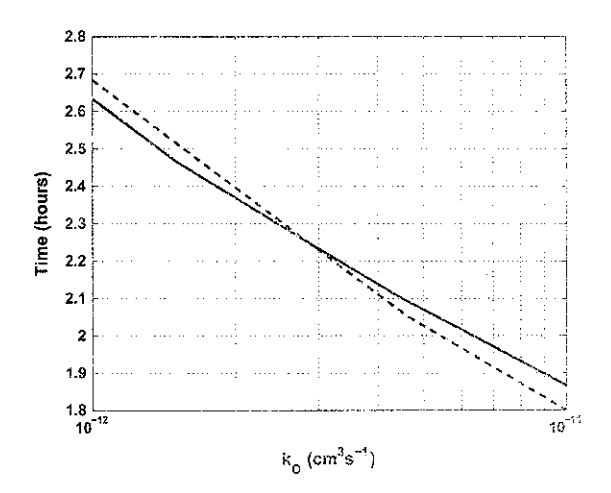


Fig. 3. (a) The temperature perturbation at 250 km as a function of the cometary  $H_2O$  production rate. (b) The ratio of H densities in the perturbed and unperturbed atmospheres as a function of cometary  $H_2O$  production rate.

drive strong vertical and/or horizontal winds, modifying the energy balance in the atmosphere. Thus, the results for these large production rates should not be interpreted quantitatively but do indicate that the perturbations to the atmosphere would be extreme.

Fig. 9 shows how the time constant for the decay of the temperature perturbation depends on the  $O-CO_2$  de-excitation rate. The dependence, in fact, is quite weak. This indicates that the rate at which energy is lost from the upper atmosphere (above 150 km) is limited primarily by thermal conduction, with the efficiency of the radiative processes playing only a minor role. The time constants for the decay of the thermal perturbation depends only weakly on the size of the perturbation. For production rates of  $3 \times 10^{27}$  and  $3 \times 10^{28}$  we calculate time constants that differ by only a few percent from the value quoted above for a production rate of  $10^{28} \, \mathrm{s}^{-1}$ .



**Fig. 9.** The e-folding thermal relaxation timescale versus O+CO $_2$  de-excitation rate for a comet production rate of  $10^{28}$  s<sup>-1</sup> (solid line) and  $3\times10^{28}$  s<sup>-1</sup> (dashed line)

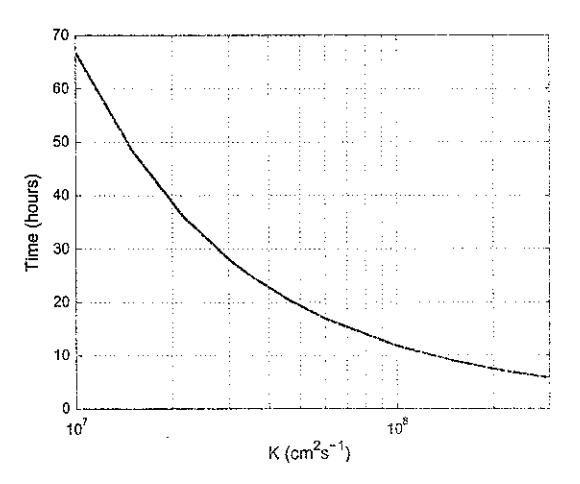


Fig. 10. The e-folding relaxation timescale for the H density distribution versus the eddy diffusion coefficient for a comet production rate of  $10^{28} \, {\rm s}^{-1}$ .

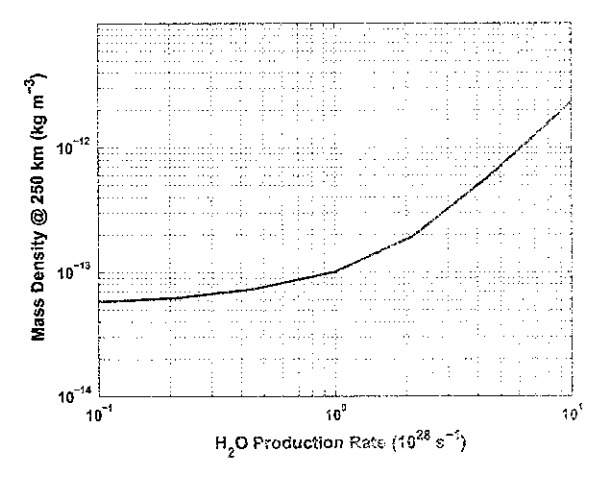


Fig. 11. The mass density of the atmosphere at 250 km as a function of the cometary  $\rm H_2O$  production rate. The increased density associated with heating of the atmosphere by the coma influx will cause increase drag on orbiting spacecraft.

The eddy diffusion coefficient is another uncertain parameter in models for the upper atmosphere of Mars. In these 1D models the eddy diffusion coefficient represents mixing processes due to both large scale motions and atmospheric waves (Bougher et al., 1999, 2000; González-Galindo et al., 2009). Fig. 10 shows the dependence of the relaxation time for the H density perturbation as a function of the eddy diffusion coefficient. Here, the dependence is quite strong, varying from 65 h to 6 h for K varying from  $10^7 \, \mathrm{cm}^{-2} \, \mathrm{s}^{-1}$  to  $3 \times 10^8 \, \mathrm{cm}^{-2} \, \mathrm{s}^{-1}$ . The eddy diffusion coefficient has a strong affect on the altitude profile of minor constituents in steady-state models but its effects can be difficult to separate from similar effects produces by an escape flux, or by chemical sources and sinks in the atmosphere. Thus, determination of this time constant would provide a useful constraint on these processes. As with the temperature perturbation, the time scales for decay of the H perturbation is essentially independent of the cometary 8-0 production rate for the range of parameters considered here.

### 5. implications for observations

The perturbations discussed above may be observable with current and future spacecraft at Mars or with HST. The most straightforward approach is to monitor the atmospheric drag on orbiting spacecraft. Of the currently active missions the Mars Reconnaisance Orbiter (MRO) has a periapse altitude of 250 km and the recently launched Mars Volatile and Evolution (MAVEN) spacecraft is planned to have a periapse altitude for most of the mission of 150 km, MAVEN is due to arrive at Mars on September 19, 2014, roughly one month before Siding Spring. The orbital periods of MRO and MAVEN are 3 and 4.5 h, respectively, slightly longer than the thermal time constants calculated here but much shorter than the H density time constant. Fig. 11 shows the enhancement in mass density at 250 km due to the comet as a function of the HoO production rate. Our model predicts that drag forces on orbiting spacecraft would increase by factors of 1.6 to 40 at 250 km for H<sub>2</sub>O production rates of  $10^{28}$ – $10^{29}$  cm<sup>-2</sup>. Atmospheric densities near 150 km are affected far less strongly, increasing by only 20% for an H<sub>2</sub>O production rate of 10<sup>29</sup> cm<sup>-2</sup>. Of course, the MAVEN orbit will be affected by increased drag at the higher altitudes and these can be used to infer density changes (Forbes et al., 2008), thus we expect that both MRO and MAVEN could sense changes in the atmosphere due to cometary input.

MAVEN also carries an ion-neutral mass spectrometer (NGIMS, Mahaffey et al., 2014) that could yield interesting constraints on the martian upper atmosphere and ionosphere. Currently, the NGIMS cover is scheduled for release 2 days before the comet encounter. Measurements of CO<sub>2</sub> density can be analyzed to determine the temperature profile of the atmosphere to search for perturbations due to the comet. NGIMS cannot measure H or H+ but the effect of increased H density should be apparent in the ionospheric composition. Recently Matta et al. (2013) have shown that the ionospheric composition of Mars depends sensitively on the H and H<sub>2</sub> density in the atmosphere, and species such as HCO\* should respond strongly to H density variations. The variations in H density due to the comet input provide an ideal opportunity to test this theory.

The increased H abundance may also be directly detectable through H Lyman alpha observations of Mars either with HST or the UV spectrometer on MAVEN. Because H Lyman alpha is optically thick to altitudes above the exobase, increased H in the upper atmosphere will appear primarily as an increased in the size of the H corona rather than an increase in brightness. A factor of 2 increase in the exobase density implies that the altitude of unit optical depth at line center will move upward by about 300 km.

#### 6. Summary and conclusions

The impact of H<sub>2</sub>O from the coma of Comet C/2013 A1 Siding Spring on Mars will cause significant perturbations of the upper atmosphere if the cometary production rate is of order 10<sup>20</sup> s<sup>-1</sup> or larger. The 293 eV H2O molecules will penetrate to the  $6.5\times10^{-5}~\mu bar$  level or roughly 150 km, which is in the thermosphere. Our 1D model for the atmospheric structure products that the H density in the thermosphere will approximately double and the temperature increase by ~30 K for a production rate of  $10^{28} \, s^{-1}$ . The temperature perturbations will persist for  $\sim 2 \, h_{\odot}$  but the H density perturbation for ~10 h. Larger comet production rates will cause larger perturbations, with essentially the same time constants. For production rates of 10<sup>29</sup> s<sup>-1</sup> the model predicts that the temperature of the upper atmosphere will increase to over 500 K, which is so large that a 1D model is likely no longer applicapriate. It does indicate however that the largest likely HyO production rates can cause extreme perturbations to the approsphere. Drag forces at 250 km on orbiting spacecraft increase by factors of 1.6 to 40 for production rates from 10<sup>28</sup> to 10<sup>29</sup> s<sup>-1</sup>, but drag forces at 150 km increase by only 20% for a production rate of  $10^{29} \, \text{s}^{-1}$ .

If the production rate of Comet Siding Spring is large enough to cause observable perturbations, more comprehensive models will be required, including 3-D effects, more sophisticated energy deposition calculations, etc. The models presented here demonstrate that perturbations to the atmosphere can be significant and can persist for significant lengths of time. Future observations of Comet Siding Spring can constrain production rates and come composition, allowing the response in the martian upper atmosphere to be a probe of the processes controlling its thermospheric structure.

# Acknowledgments

We acknowledge helpful discussion with Dr. S. Bougher. Contributions of R.V.Y. and S.M. were supported by the funds from the MAVEN project. A.M. contribution was supported by the Belgian Federal Science Policy Office and the European Space Agency (ESA, PRODEX program, contracts C 90268, 90113, and 17645), the 'Interuniversity Attraction Poles' programme financed by the Belgian government (Planet TOPERS), and by a grant from the Belgian American Education Foundation (BA6F). S.M.H. was supported by NSF Astronomy and Astrophysics Postdoctoral Fellowship AST-1102827.

#### References

- A'Hearn, M.F., Millis, R.C., Schleicher, D.O., Osip, D.J., Birch, P.V., 1995. The ensemble properties of comets: Results from narrowband photometry of 85 comets, 1976–1992. Icarus 118, 223–270.
- Anicich, V., 1993. Evaluated bimolecular ion-molecule gas phase kinetics of positive ions for use in modeling planetary atmospheres, cometary comae, and interstellar clouds. J. Phys. Chem. Ref. Data 22, 1469–1569.
- Bank, P.M., Kockarts, G., 1973. Aeronomy A. Academic Press, New York, 1973.
   Baulch, D. et al., 2005. Evaluated kinetic data for combustion modeling: Supplement ii. J. Phys. Chem. Ref. Data 34 (3), 757-1397.
- Bougher, S.W., Engel, S., Roble, R.G., Foster, B., 1999. Comparative terrestrial planet thermospheres 2. Solar cycle variation of global structure and winds at equinox. J. Geophys. Res. 104, 16591–16611.
- Bougher, S.W., Engel, S., Roble, R.G., Foster, B., 2000. Comparative terrestrial planet thermospheres 3. Solar cycle variation of global structure and winds at solstices. J. Geophys. Res. 105 (E), 17669–17692.
- Bougher, S.W., Roble, R.G., Fuller-Rowell, T., 2002. Simulations of the Upper Atmospheres of the Terrestrial Planets. Washington DC American Geophysical Union Geophysical Monograph Series 130, p. 261.
- Union Geophysical Monograph Series 130, p. 261.
  Caridade, P., Rodrigues, S., Sousa, F., Varandas, A., 2005. Unimolecular and bimolecular calculations for NH<sub>2</sub>, J. Phys. Chem. A 109, 2356–2363.
- Castle, K.J., Black, i.A., Simione, M.W., Dodd, J.A., 2012. Vibrational relaxation of  $CO_2(v_2)$  by  $O(^3P)$  in the 142–490 K temperature range, J. Geophys. Res. (Space Phys.) 117, 4310.

- Chaufray, J.Y., Bertaux, J.-L., Leblanc, F., Quémerais, E., 2008. Observations of the hydrogen corona with SPICAM on Mars Express. Icarus 195, 598-613.
- Chaufray, J.Y., Leblanc, F., Quémerais, E., Bertaux, J.L., 2009. Martian oxygen density at the exobase deduced from O I 130.4-nm observations by Spectroscopy for the investigation of the characteristics of the atmosphere of Mars on Mars Express. J. Geophys. Res. (Planets) 114, 2006.
- Dalgarno, A., Smith, F.J., 1962. The thermal conductivity and viscosity of atomic oxygen. Planet. Space Sci. 9 (1), 1-2.
- oxygen, Planet, Space Sci. 9 (1), 1–2.
  Feofilov, A.G., Kutepov, A.A., She, C.-Y., Smith, A.K., Pesnell, W.D., Goldberg, R.A., 2012. COtextsubscript2(1)–0 quenching rate coefficient derived from coincidental SABER/TIMED and Fort Collins lidar observations of the mesosphere and lower thermosphere. Atmos. Chem. Phys. 12, 9013–9023.
- Fink, U., 2009. A taxonomic survey of comet composition 1985–2004 using CCD spectroscopy. Icarus 201, 311–334.
- Forbes, J.M., Lemoine, F.G., Bruinsma, S.L., Smith, M.D., Zhang, X., 2008, Solar flux variability of Mars' exosphere densities and temperatures. Geophys. Res. Lett. 35, 1201.
- Forget, F. et al., 2009. Density and temperatures of the upper martian atmosphere measured by stellar occultations with Mars Express SPICAM. J. Geophys. Res. (Planets) 114, 1004.
- Geppert, W. et al., 2005. Dissociative recombination branching ratios and their influence on interstellar clouds. J. Phys.: Conf. Ser. 4, 26–31.
- González-Galindo, F., López-Valverde, M.A., Angelats i Coll, M., Forget, F., 2005. Extension of a martian general circulation model to thermospheric altitudes: UV heating and photochemical models. J. Geophys. Res. (Planets) 110, 9008.
- González-Galindo, F., Forget, F., López-Valverde, M.A., Angelats i Coll, M., 2009. A ground-to-exosphere martian general circulation model: 2. Atmosphere during solstice conditions – Thermospheric polar warming, J. Geophys. Res. (Planets) 114, 8004.
- Harrington, J. et al., 2004, Lessons from shoemaker-levy 9 about Jupiter and planetary impacts. In: Bagenal, F., Dowling, T., McKinnon, W. (Eds.), Jupiter: The Planet, Satellites and Magnetosphere. Cambridge University Press, Cambridge, UK, pp. 159–184.
- Huestis, D.L. et al., 2008. Cross sections and reaction rates for comparative planetary Aeronomy, Space Sci. Rev. 139 (1), 63~105.
- Johnson, R.E., 1990. Energetic Charged-Particle Interactions with Atmospheres and Surfaces. Springer-Verlag, Berlin.
- Leblanc, F., Chaufray, J.Y., Lilensten, J., Witasse, O., Bertaux, J.-L., 2006. Martian dayglow as seen by the SPICAM UV spectrograph on Mars Express, J. Geophys. Res. (Planets) 111. 9.
- Le Padellec, A., Sheehan, C., Talbi, D., Mitchell, J., 1997. A merged-beam study of the dissociative recombination of HCO\*, J. Phys. B: Atmos. Mol. Opt. Phys. 30, 319– 327.
- Lopez-Puertas, M., Lopez-Valverde, M.A., 1995. Radiative energy balance of CO<sub>2</sub> non-LTE infrared emissions in the martian atmosphere, Icarus 114, 113.
- Matta, M., Withers, P., Mendillo, M., 2013. The composition of Mars' topside ionosphere: Effects of hydrogen. J. Geophys. Res. (Space Phys.) 118 (5), 2681– 2693
- McEwan, M., Anicich, V., 2007. Titan's ion chemistry: A laboratory perspective. Mass Spectrom. Rev. 26 (2), 281–319.
- Mitchell, J., 1990. The dissociative recombination of molecular ions. Phys. Rep. 186, 215–248.
- Muł, P., McGowan, J., Defrance, P., Mitchell, J., 1983. Merged electron-ion beam experiments: V. dissociative recombination of OH\*, H<sub>2</sub>O\*, H<sub>3</sub>O\* and D<sub>3</sub>O\*, J. Phys. B: Atmos. Mol. Phys. 16, 3099–3107.
  Nair, H., Allen, M., Anbar, A.D., Yung, Y.L., Clancy, R.T., 1994. A photochemical model
- Nair, H., Allen, M., Anbar, A.D., Yung, Y.L., Clancy, R.T., 1994. A photochemical mode of the martian atmosphere. Icarus 111, 124–150.
- Parkinson, W.H., Rufus, J., Yoshino, K., 2003. Absolute absorption cross section measurements of CO<sub>2</sub> in the wavelength region 163~200 nm and the temperature dependence, Chem. Phys. 290, 251–256.
- Rosén, S. et al., 2000. Recombination of simple molecular ions studied in storage ring: dissociative recombination of H<sub>2</sub>O\*. Faraday Discuss. 115, 295–302.
- Sander, S., et al., 2011. Chemical kinetics and photochemical data for use in atmospheric studies, evaluation number 17. JPL Publication 10-6, Jet Propulsion Laboratory, Pasadena, CA, USA.
- Laboratory, Pasadena, CA. USA.

  Stewart, A.I.F., Alexander, M.J., Meier, R.R., Paxton, L.J., Bougher, S.W., Fesen, C.G., 1992. Atomic oxygen in the martian thermosphere. J. Geophys. Res. 97, 91–102.
- Tenishev, V., Combi, M., Davidsson, B., 2008. A global kinetic model for Cometary Comae: The evolution of the Coma of the Rosetta Target Comet Churyumov– Gerasimenko throughout the Mission. Astrophys. J. 685 (1), 659-677.
  Vesovic, V., Wakeham, W.A., Olchowy, G.A., Sengers, J.V., Watson, J.T.R., Millat, J.,
- Vesovic, V., Wakeham, W.A., Olchowy, G.A., Sengers, J.V., Watson, J.T.R., Millat, J., 1990. The transport properties of carbon dioxide. J. Phys. Chem. Ref. Data 19 (3), 763–808.
- Vuitton, V. et al., 2009. Negative ion chemistry in titan's upper atmosphere. Planet. Space Sci. 57, 1558–1572.
- Vuitton, V., Yelle, R., Lavvas, P., Klippenstein, S., 2012. Rapid association reactions at low pressure: Impact on the formation of hydrocarbons on titan. Astrophys. J. 744, 11–18.
- Wakelam, V. et al., 2012. A kinetic database for astrochemistry (kida). Astrophys. J. Suppl. Ser. 199, 21–42.
- Suppl. Ser. 199, 21-42.
  Woods, T.N. et al., 2005. Solar EUV Experiment (SEE): Mission overview and first results. J. Geophys. Res. (Space Phys.) 110, 1312.
- Ziegler, J.F., 1980. Handbook of Stopping Cross-Sections for Energetic Ions in All Elements, Pergamon Press, New York.
- Ziegler, J.F., 1984. Ion Implantation Science and Technology. Academic Press, Orlando.